Journal of Alloys and Compounds 508 (2010) 433–439

Contents lists available at ScienceDirect

Journal of Alloys and Compounds

journal homepage: www.elsevier.com/locate/jallcom

Nanocrystalline Mn–Zn ferrites from mixed oxalates: Synthesis, stability and magnetic properties

A. Angermann [a], J. Töpfer [a,*], K.L. da Silva [b], K.D. Becker [b]

[a] University of Applied Sciences, Dept. SciTec, Carl-Zeiss-Promenade 2, 07745 Jena, Germany
[b] Institute of Physical and Theoretical Chemistry, Technische Universität Braunschweig, Hans-Sommer-Str. 10, 38106 Braunschweig, Germany

ARTICLE INFO

Article history:
Received 21 April 2010
Received in revised form 12 August 2010
Accepted 24 August 2010

Keywords:
Ferrites
Oxalates
Powder morphology

ABSTRACT

Nanocrystalline Mn–Zn ferrite spinel powders were synthesized by thermal decomposition of mixed β-(Mn, Zn, Fe)$(C_2O_4)\cdot 2H_2O$ oxalate. Thermolysis of the oxalate for 2 h at 300 °C in air yields an amorphous product, whereas at 400 and 500 °C ferrite spinels with unit cell parameters of 8.394(7) and 8.495(3) Å, respectively, are formed. Decomposition of the oxalate at 500 °C for 24 h results in a mixture of haematite and a Fe-poor spinel revealing the metastability of the nanocrystalline spinel at that temperature. The crystallite sizes are 12 and 45 nm for ferrite spinel powders synthesized at 400 and 500 °C, respectively. Zero ferrous ion concentrations were measured by redox titration, suggesting that the ferrites are defect spinels containing Fe^{3+} and cation vacancies. Thermal analysis and XRD demonstrate that the ferrites undergo several phase transitions during annealing in air.

Magnetic measurements reveal that the saturation magnetization at 5 K of the ferrites increases with crystallite size. Hysteresis loops measurements demonstrate superparamagnetic behavior at room temperature of the nanocrystalline powder obtained at 300 °C. Mössbauer spectroscopy at room temperature confirms the superparamagnetic character of that sample. The ferrites obtained at 400 and 500 °C, however, represent a mixture of small superparamagnetic and larger ferrimagnetic particles.

1. Introduction

Various synthesis routes for nanocrystalline oxide powders have been explored in recent years. This trend also holds for soft ferrites with the spinel structure. Spinel-type Mn–Zn ferrites are an important group of soft ferrites which are commercially used for power supplies, inductors, chokes, etc. [1]. Some of these applications require high-purity ferrites with fine-grained, dense and homogeneous microstructures. Moreover, the distribution of additives in the ppm concentration range within the ceramics microstructure is of major importance. Usually, highly reactive Mn–Zn ferrite powders are prepared by the standard mixed oxide route including intense fine milling procedures. However, powders from that process might suffer from contaminations from grinding media or unfavorable aggregation behavior, etc. Therefore, alternative synthesis routes for the preparation of non-contaminated, submicron and nanocrystalline ferrite powders were studied aiming at replacing the traditional mixed oxide ceramic process. Examples of synthesis techniques for nanocrystalline Mn–Zn ferrite powders include hydrothermal synthesis [2–4], mechano-chemical synthesis [5–7], sol–gel chemistry [8,9], combustion synthesis [10], and micro-emulsion technique [11,12]. Another promising synthesis route is the thermal decomposition of precursors coprecipitated from aqueous/alcoholic metal solutions. Several precursor routes were examined, e.g. the coprecipitation with hydroxide [13].

The synthesis of spinel-type ferrites $MeFe_2O_4$ through thermal decomposition of oxalates is a straightforward synthesis route [14], which could be easily up-scaled as batch-type process for ferrite powder fabrication. Oxalate coprecipitation was already applied for the synthesis of reactive Mn–Zn ferrite powders [15]. A modified oxalate-hydrazine precipitation technique was reported recently [16]. Angermann and Töpfer explored the synthesis of nanocrystalline Mn–Zn ferrite powders via oxalate precursors [17] and reported on the structure, morphology and thermal behavior of the mixed oxalates prepared at different precipitation conditions.

The precipitation of transition metals with oxalic acid yields oxalates that might crystallize in two different polymorphs. Ferrous oxalate dihydrate, $Fe(C_2O_4)\cdot 2H_2O$, for example, appears as α-ferrous oxalate (Humboltine) with a monoclinic unit cell, space group C2/c (No. 15), and $a_0 = 12.05$ Å, $b_0 = 5.57$ Å, $c_0 = 9.76$ Å, and $\beta = 124°18'$ ($z = 4$) or as a β-polymorph with an orthorhombic cell, space group Cccm (No. 66), with $a_0 = 12.26$ Å, $b_0 = 5.57$ Å, and $c_0 = 15.48$ Å ($z = 8$) [18]. It was shown recently, that the temperature of precipitation is a key parameter for the synthesis of either α- or β-Fe- or (Fe, Mn, Zn)-oxalates, respectively. Moreover, the

* Corresponding author. Tel.: +49 3641 205350; fax: +49 3641 205451.
E-mail address: joerg.toepfer@fh-jena.de (J. Töpfer).

0925-8388/$ – see front matter © 2010 Elsevier B.V. All rights reserved.
doi:10.1016/j.jallcom.2010.08.083

morphology of the oxalate crystals can be tailored by selecting appropriate temperatures [17,19].

The thermal decomposition of oxalates generally proceeds between 200 and 400 °C and results in oxide powders, if performed in oxygen-rich atmospheres. Ferrous oxalate decomposes in air to form haematite, α-Fe_2O_3 [20,21] and the thermolysis of mixed oxalates results in ternary oxides, e.g. ferrites [14]. It was shown, that in some cases the thermolysis of mixed oxalates might lead to the formation of metastable spinels. For example, decomposition of Ni–Mn-oxalates at 350 °C results in the formation of Ni–Mn spinels rather than a mixture of $NiMnO_3$ and Mn_2O_3 which would have been the expected equilibrium products at that temperature [22]. The nanocrystalline Ni–Mn spinels are nonstoichiometric, e.g. $NiMn_2O_{4+\delta}$, and the deviation from stoichiometry is accommodated as cation vacancies (V), i.e. $Ni_{4/(4+\delta)}Mn_{8/(4+\delta)}V_{3\delta/(4+\delta)}O_{4.00}$. On the other hand, it is essential to decompose oxalate mixed crystals to synthesize ternary (or multi-component) oxides: the mixed oxalate $NiMn_2(C_2O_4)_3{\cdot}6H_2O$ transforms into metastable $NiMn_2O_{4+\delta}$ spinel at 350 °C in air, whereas a mixture of Ni- and Mn-oxalates forms a mixture of binary oxides at the same conditions [23].

In this communication we report on the synthesis and properties of nanocrystalline Mn–Zn ferrites. Thermal decomposition of mixed oxalates in air at 300, 400 and 500 °C leads to ferrite powders with crystallite sizes of 5–50 nm. We report on the phase stability and magnetic properties of these ferrites.

2. Experimental

Mn–Zn–Fe oxalate hydrate crystals of composition $Mn_{0.686}Zn_{0.233}Fe_{2.081}(C_2O_4)_3{\cdot}6H_2O$ were prepared by precipitation at room temperature from aqueous metal ion solutions with oxalic acid in an argon atmosphere. Iron powder (p.a. grade, Merck, Germany) as starting material was dissolved in an acetic acid solution under argon. Mn- and Zn-acetate hydrates (Mn- and Zn-contents determined gravimetrically) were also dissolved. After precipitation, the suspension of mixed oxalates was dried at 60 °C in a vacuum rotary evaporator in air. The oxalates were calcined for 2 h in air at 300, 400, and 500 °C, respectively, in flat Pt crucibles without lids.

Powder X-ray diffraction measurements (XRD) were performed with a Siemens D5000 using Cu Kα radiation (step time 8 s; step size 0.02°; 10–130° 2θ). Lattice parameters were refined using the TOPAS R software package (Bruker AXS, Karlsruhe, Germany). The specific surfaces A_s of the powders were determined by nitrogen adsorption (BET, Nova 2000, Quantachrome Instruments, Boynton Beach, USA); a mean particle size was estimated using the relation $d_{BET} = 6/\rho A_s$ with the density ρ. The mean crystallite size d_{XRD} was estimated from XRD line broadening using the Scherrer equation, $d_{XRD} = K\lambda/[(B-b)\cos\theta]$, with the wavelength λ, the peak width B, the instrumental broadening b ($b = 0.08°$ for standard LaB_6), the Bragg angle θ and the shape factor $K \approx 0.89$.

The ferrite particles were investigated by Scanning Electron Microscopy SEM (DSM 940A, Zeiss, Jena, Germany). Transmission electron microscopy (TEM) studies were performed with a JEM 3010 (Jeol, Japan). Thermal analysis (TG, DTA) was carried out with a SETARAM TGA92 system, the samples were heated in open Pt containers (TG + DTA sample holder: diameter 3 mm, height 6 mm) in air with a rate of 2 K/min (sample mass about 20 mg). The Fe^{2+}-concentration in the ferrite powders was determined by cerimetric redox titration after dissolving the sample in hydrochloric acid under argon. The Fe^{2+} was titrated with a 0.05 N Ce^{4+} solution under a flow of argon with potentiometric detection of the equivalent point. The detection limit of that titration is given by the first drop of Ce^{4+} solution ($V \approx 0.03$ ml), which corresponds to 0.08 wt% Fe^{2+} for 100 mg of a ferrite sample.

Magnetic properties were measured with a Quantum Design SQUID magnetometer. Hysteresis loops $M(H)$ were measured at 5 and 298 K. The magnetization at the maximum field of 50 kOe was taken as saturation magnetization M_s. The magnetization was also recorded as function of temperature $M(T)$ between 5 and 400 K in zero-field-cooled (ZFC) and field-cooled (FC, $H = 100$ Oe) modes, respectively. Mössbauer measurements were carried out in transmission mode at room temperature using a conventional microcomputer controlled spectrometer (Halder) in sinusoidal mode. A ^{57}Co in Rh radiation source was used for measurements. For the quantitative analysis of the Mössbauer spectra the Recoil spectral analysis software was employed [24].

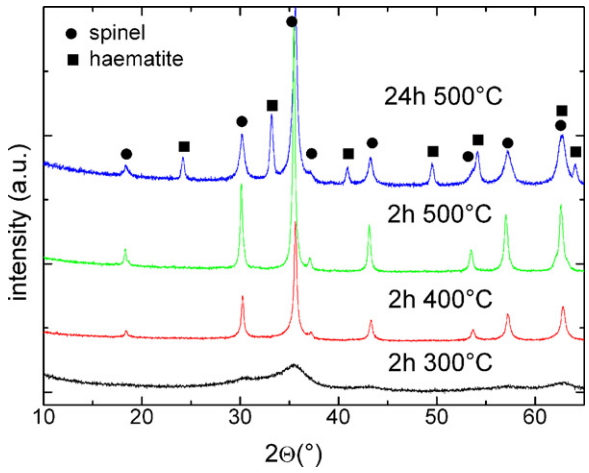

Fig. 1. XRD patterns of the oxide powders obtained by thermal composition of Mn–Zn–Fe mixed oxalate at 300, 400, and 500 °C for 2 h and at 500 °C for 24 h in air.

3. Results and discussion

The Mn–Zn–Fe oxalate hydrate precipitated at room temperature is a yellowish powder. X-ray diffraction studies show that the orthorhombic β-oxalate with lattice parameters $a_0 = 12.241(9)$ Å, $b_0 = 5.567(4)$ Å, and $c_0 = 15.480(9)$ Å has formed [17]. The thermal decomposition of the mixed oxalate hydrate in air is almost complete at 300 °C. The DTA curve exhibits an endothermic peak at 150 °C as signature of the dehydration step and an exothermic peak at 240 °C corresponding to the oxalate decomposition reaction [17]. The total mass loss is 57% at 500 °C, which agrees well with a calculated loss of 56.9% for the decomposition reaction:

$$Mn_{0.686}Zn_{0.233}Fe_{2.081}(C_2O_4)_3 \cdot 6H_2O + \frac{1}{2}O_2 \rightarrow Mn_{0.686}Zn_{0.233}Fe_{2.081}O_4 + 3CO + 3CO_2 + 6H_2O \quad (1)$$

Samples of the mixed oxalate were decomposed at 300, 400, 500, and 750 °C for 2 h in air, respectively. XRD analysis of the decomposition products (Fig. 1) demonstrates that the oxide formed at 300 °C is not well crystallized yet. However, very broad peaks with low intensities indicate that very small crystallites of a spinel-type lattice have formed. XRD patterns of the samples prepared at 400 and 500 °C reveal the formation of single-phase spinel-type ferrites with lattice parameters of 8.394(7) and 8.495(3) Å, respectively. The unit cell parameter of the ferrite formed at 500 °C agrees well with data reported for this particular Mn–Zn ferrite [6]. On the other hand, the lattice constant of the sample synthesized at 400 °C is rather small indicating that the spinel is cation defective and/or that at these conditions the crystallization of a homogeneous spinel ferrite is not completed yet.

The formation of spinel ferrites at the low temperatures of our study is rather unexpected. Spinel-type ferrites in the system Mn–Zn–Fe–O in air are stable at high temperatures only and decompose into a mixture of haematite, α-Fe_2O_3, and a Fe-poor spinel during cooling [25,26]. To test for the metastability of the spinel ferrite at 500 °C, a sample of the mixed oxalate was annealed at 500 °C for 24 h. In that case, we indeed observed the expected mixture of haematite/spinel (Fig. 1). This confirms that the ferrite formed after oxalate decomposition at 500 °C for 2 h is a metastable spinel and transforms into the thermodynamically stable state under prolonged annealing.

The morphological properties of the oxide powders are summarized in Table 1. The powder synthesized at 300 °C exhibits a

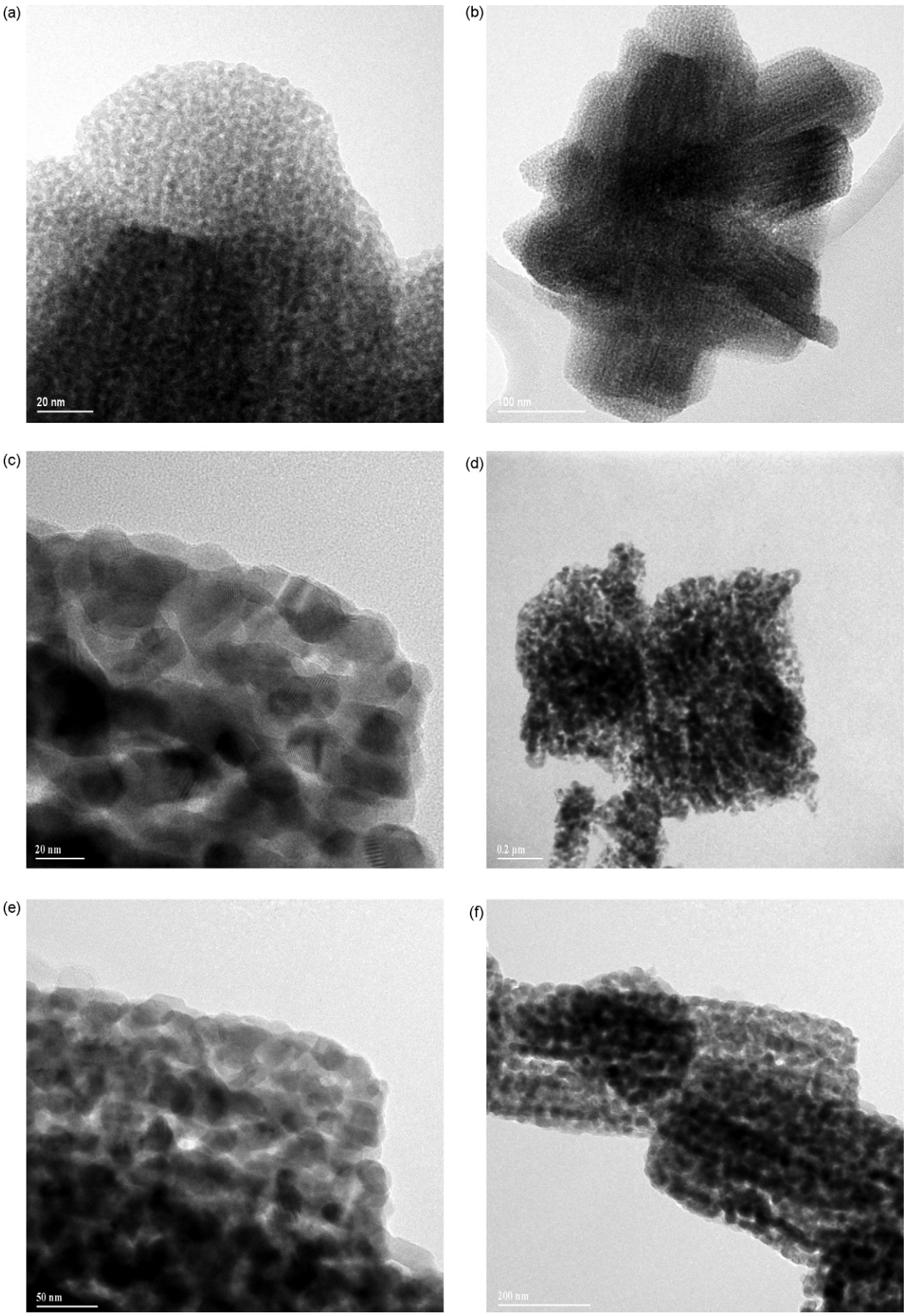

Fig. 2. TEM micrographs of powders prepared by thermal decomposition of β-Mn–Zn–Fe mixed oxalates, respectively, at 300 °C (a and b), 400 °C (c and d), and 500 °C (e and f).

Table 1
Properties of oxide powders obtained by thermal decomposition of β-Mn–Zn–Fe oxalates at 300–750 °C in air (specific surface area A_s, particle diameter from specific surface d_{BET}; mean crystallite size d_{XRD}; lattice parameter a_0; ferrous concentration and saturation magnetization M_s at 5 K).

T (°C)	A_s (m²/g)	d_{BET} (nm)	d_{XRD} (nm)	Phases (XRD)	a_0 (Å)	Fe^{2+} (wt%)	M_s (emu/g)
300 °C/2h	235	5	–	Spinel	–	–	21.3
400 °C/2h	85	14	12 ± 2	Spinel	8.394(7)	0.02	61.7
500 °C/2h	40	50	45 ± 4	Spinel	8.495(3)	0.05	66.1
750 °C/2h	2	570	–	Haematite and spinel	–	–	–

large specific surface that corresponds to a particle size of about d_{BET} = 5 nm. TEM micrographs of this powder (Fig. 2a and b) confirm that the individual particles are few nanometers in size, but form aggregates of 100–200 nm in size. The ferrite powder obtained after calcination at 400 °C for 2 h consists of larger particles with d_{BET} = 14 nm. From the XRD peak broadening an average crystallite size of d_{XRD} = 12 nm was estimated. TEM micrographs (Fig. 2c and d) confirm that nanosize particles were synthesized. Calcination at 500 °C results in particles of crystallite size of d_{XRD} = 45 nm. From BET measurements a mean particle size d_{BET} = 50 nm results. TEM micrographs (Fig. 2e and f) show that the individual particles are aggregated to form loose aggregates with a size of several hundred nanometers. SEM micrographs (not shown here) demonstrate that the powder consist of loose aggregates of 1–2 μm size. The aggregate size and shape of the oxide particles is predetermined by the oxalate morphology: mixed β-oxalate crystals (precipitated at 20 °C) exhibit a similar aggregate size as their decomposition products at 300 °C [17,19]. As expected, the particle size increases to sub-micron size after oxalate decomposition at 750 °C (Table 1).

The ferrous concentrations, measured by cerimetric titration, are also shown in Table 1. If the composition of the Mn–Zn ferrite would be that of a stoichiometric ferrite, a considerable concentration of ferrous ions $Mn^{2+}_{0.686}Zn^{2+}_{0.233}Fe^{2+}_{0.081}Fe^{3+}_{2}O_4$ would be required (theor. 1.94 wt% Fe^{2+}). Under more oxidizing conditions all Fe ions are accommodated as ferric ions and the spinel composition corresponds to $Mn^{2+}_{0.679}Zn^{2+}_{0.231}V_{0.030}Fe^{3+}_{2.060}O_4$ including a significant concentration of cation vacancies. If the possibility of complete oxidation of Mn^{2+} ions is also taken into account, a highly oxidized defect spinel results with the limiting composition $Mn^{3+}_{0.626}Zn^{2+}_{0.213}V_{0.262}Fe^{3+}_{1.899}O_4$. The measured small Fe^{2+} concentrations, see Table 1, indicate that the ferrites produced in our study are nonstoichiometric with a significant concentration of cation vacancies. Cation-deficient defect spinels as a result of low-temperature synthesis have already been reported for several systems, e.g. $Fe_{3-x}Mn_xO_4$ [27] and $NiMn_2O_4$ [22].

The thermal behavior of the nanocrystalline Mn–Zn ferrite defect spinel during heating in air was monitored by thermal analysis. The rather complex thermal behavior of a ferrite powder which

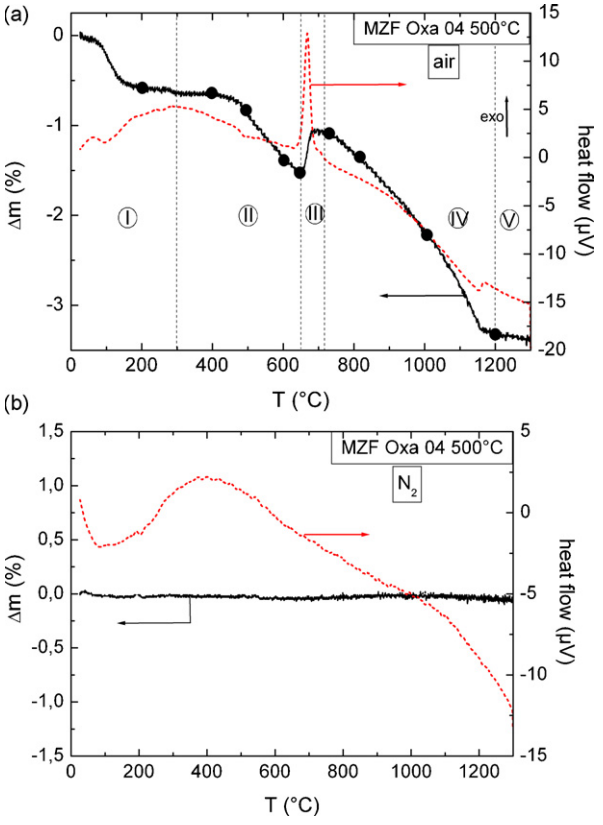

Fig. 3. TG and DTA curves of a nanocrystalline Mn–Zn ferrite powder (obtained by oxalate decomposition at 500 °C for 2 h) annealed in air (a) and nitrogen (b) with 10 K/min; (black dots on the TG curve correspond to annealing temperatures for XRD study).

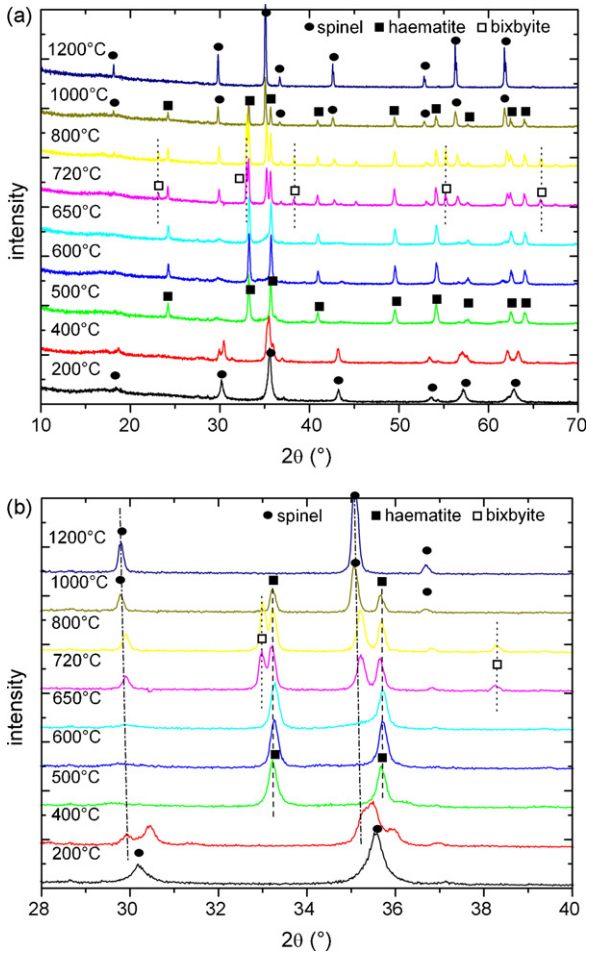

Fig. 4. XRD patterns of the nanocrystalline Mn–Zn ferrite annealed at different temperatures for 4 h in air and quenched (a) and expanded view of diffraction angles between 28 and 40° (b).

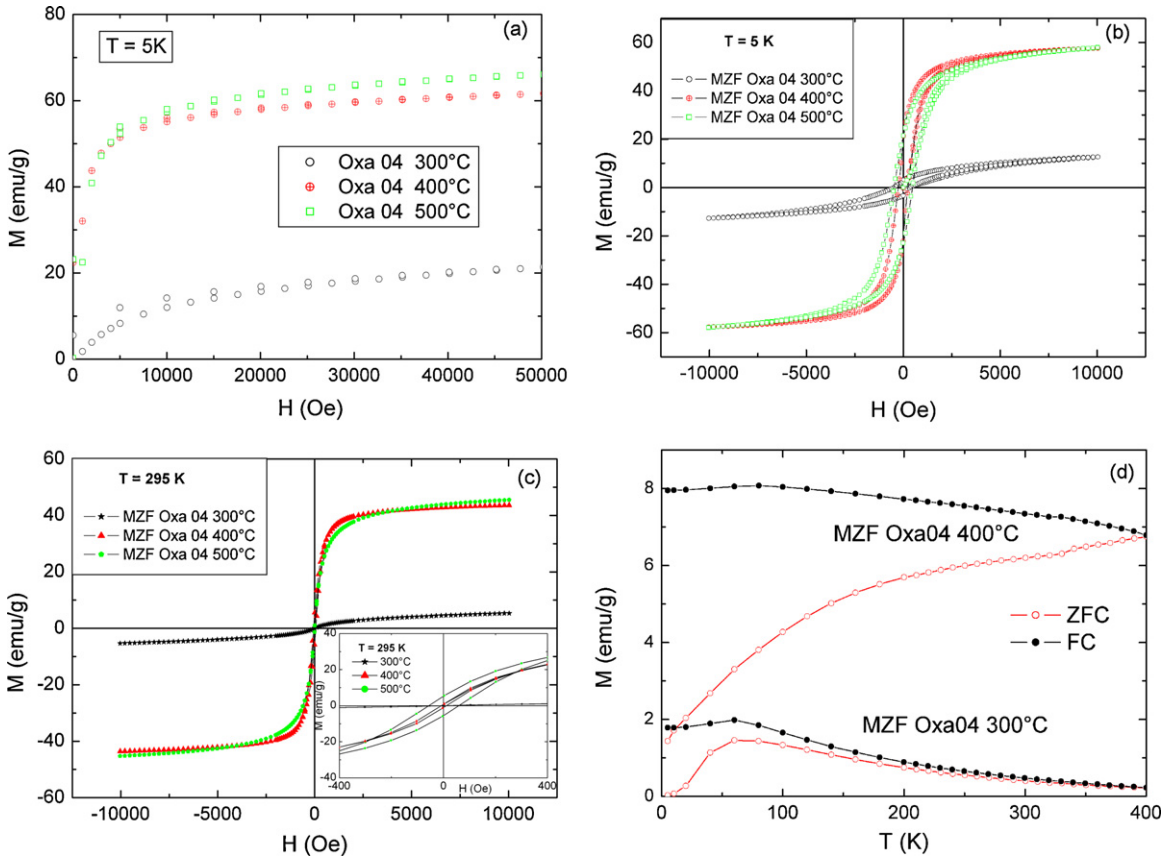

Fig. 5. Magnetic properties of nanocrystalline ferrite powders prepared by thermal decomposition of oxalates at 300, 400 and 500 °C: magnetization vs. field at 5 K (a); hysteresis loops at 5 K (b) and at 295 K (c); inset: hysteresis loops from −400 to +400 Oe); and magnetization vs. temperature (field-cooled FC and zero-field-cooled ZFC curves) of ferrite powders 300 and 400 °C (d).

was prepared by oxalate calcination at 500 °C for 2 h is subdivided into five sections (Fig. 3a). In order to elucidate the series of phase transformations, samples of the defect spinel were annealed at given temperatures (marked by dots in the TG curve in Fig. 3a) for 4 h and quenched from that temperature. The XRD patterns of the products are shown in Fig. 4. At low temperatures (section I) the nanocrystalline ferrite powder loses some weight due to removal of adsorbates. The X-ray diffractogram of the powder annealed at 200 °C still exhibits reflections of a single-phase spinel. In section II, between 300 and 650 °C a mass loss of about 0.85% is observed. This indicates that a fraction of the Mn ions in the defect spinel has an oxidation state higher than +2 and that reduction of Mn^{3+} seems to set in at 500 °C. The reduction of Mn ions to Mn^{2+} in that temperature range has also been reported for spinels of the Mn–Fe–O system [28]. Correspondingly, XRD suggests that this reduction process is accompanied by phase transformations. Whereas at 200 °C a single-phase spinel exists, the reaction product at 400 °C appears to consist of two spinels. This can be very well recognized by the splitting of the (2 2 0) reflection at $2\theta = 30°$ (Fig. 4b), because there is no overlap with peaks of other phases. At 500, 600, and 650 °C the X-ray diffractograms of the quenched samples are characterized by haematite as main phase in combination with a minority spinel ferrite. A similar series of transitions was reported for the oxidation of a stoichiometric Mn–Zn ferrite between 200 and 600 °C in air in a combined Mössbauer and XRD study [29]. In this study the authors discovered the formation of a mixture of a Mn ferrite with a large concentration of cation vacancies and a Zn-rich Mn ferrite at 300 °C for 6 h in air. At 500 °C the defective Mn ferrite has transformed into haematite, coexisting with the spinel ferrite. Therefore, we conclude that in section II the defect Mn–Zn spinel ferrite decomposes into two spinels; one being a defective spinel ferrite which is transformed into α-$(Fe/Mn)_2O_3$ during further heating and the other one being an iron-poor Mn–Zn ferrite. This is also consistent with the fact that Mn–Zn–Fe oxalate calcined at 500 °C for 24 h results in a mixture of haematite and spinel ferrite (Fig. 1).

In section III, between 650 and 720 °C, the TG signal shows a mass gain which is accompanied by a large exothermic DTA signal. This process is due to oxidation of Mn^{2+} [27,30]. The XRD pattern of the sample heated to 720 °C (Fig. 4) exhibits reflections of three coexisting major phases: haematite, spinel ferrite, and bixbyite, α-Mn_2O_3. Further increase of temperature reveals again a loss of mass between 720 and 1180 °C (section IV in Fig. 3a). The corresponding XRD patterns of the samples quenched from 800 to 1000 °C demonstrate that in section IV the three compounds, which were formed in section III, again react to form a single Mn–Zn ferrite phase. At 1000 °C bixbyite has disappeared and the residual concentration of haematite is decreased. At 1180 °C the single-phase spinel ferrite field (section V) is entered, as evidenced by a small DTA peak and a stable mass signal (Fig. 3a). Indeed, the sample quenched from 1200 °C is single-phase ferrite according to XRD (Fig. 4). A similar thermogravimetric behavior has been reported for Mn–Zn ferrite nanocrystals prepared by a hydrothermal process [4]. If the thermal analysis is performed by heating the defect spinel ferrite in a nitrogen atmosphere (Fig. 3b) the mass remains constant up to 1300 °C. This suggests that the complex series of phase transitions observed in air does not occur under reduced partial pressure of oxygen. Under these conditions, the stability field of the spinel fer-

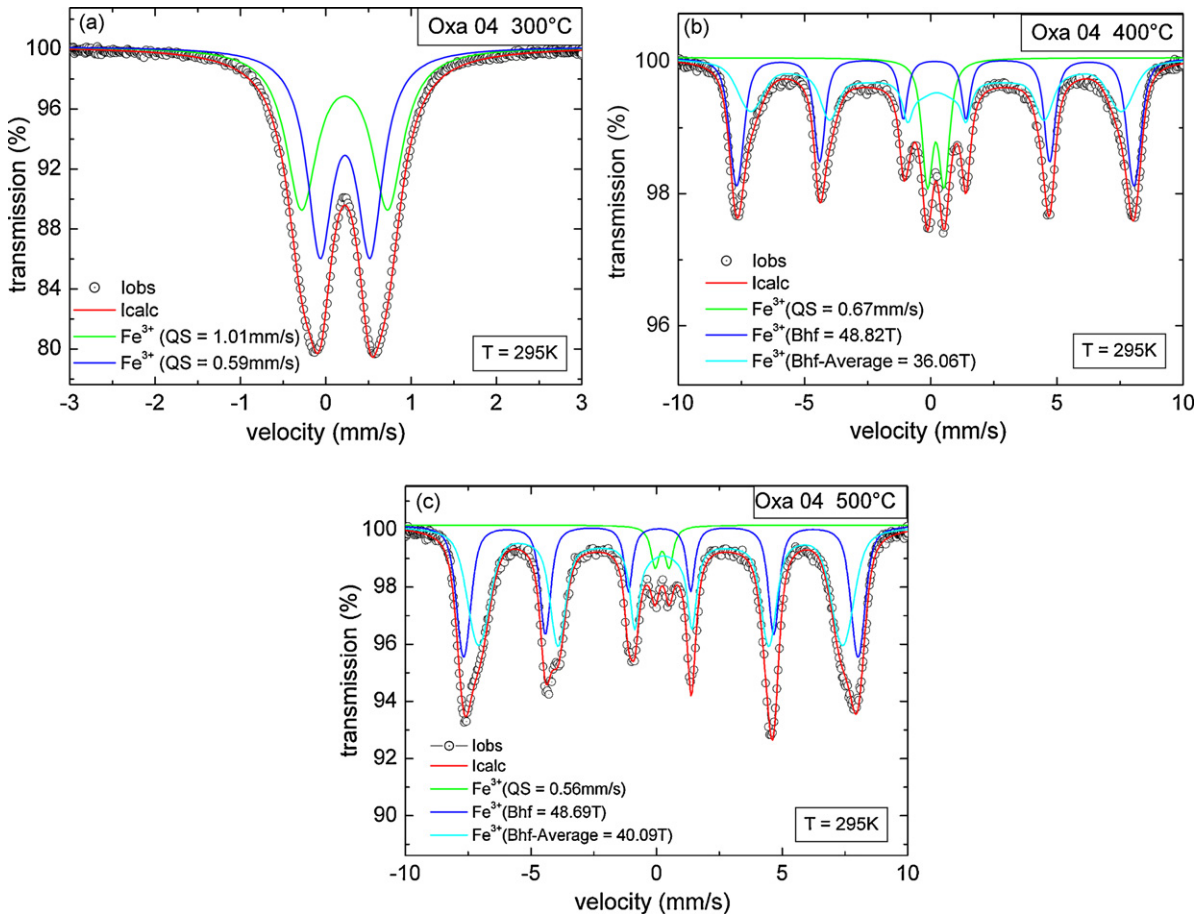

Fig. 6. Room temperature Mössbauer spectra of nanocrystalline ferrite powders prepared by thermal decomposition of oxalates at 300, 400, and 500 °C: measured spectra (circles), modeled components (blue and green) and summation spectra (red). (For interpretation of the references to color in this figure legend, the reader is referred to the web version of the article.)

rite is expanded from high temperatures down to temperatures as low as 400 °C.

The magnetization of the ferrite powders obtained by thermal decomposition of oxalates at 300, 400, and 500 °C as a function of magnetic field is shown in Fig. 5a. The magnetization of all samples is not completely saturated yet at the maximum field of the measurements (50 kOe). The saturation magnetization M_s increases with the crystallite size of the ferrite particles (Table 1). The M_s values of all prepared nanocrystalline Mn–Zn ferrites, however, are significantly lower than the saturation magnetization of the bulk ferrite with M_s = 140 emu/g [31]. The reduced M_s values are related to the formation of a surface layer of reduced magnetization which might be caused by a different composition and/or cation distribution or disordered spins within a surface layer. Recently, a detailed model has been put forward for the reduced magnetization observed for nanosized $NiFe_2O_4$ particles [32]. The hysteresis loops of the ferrite powders prepared at 300, 400, and 500 °C measured at 5 and 295 K in fields up to 10 kOe are shown in Fig. 5b and c. At T = 5 K, all three samples show ferrimagnetic behavior; the magnetizations are not saturated yet at 10 kOe, but the magnetizations observed at 10 kOe already exhibit the reported trend with particle size. The samples display hysteresis behavior with a significant coercive field. In comparison, hysteresis loops at room temperature (Fig. 5c) are much thinner. Closer inspection (inset of Fig. 5c) reveals that only the sample prepared at 300 °C exhibits zero coercivity and, thus, is superparamagnetic at 295 K. The samples prepared at 400 and 500 °C display small, but non-zero coercivities with H_c increasing with particle size. This indicates that in these ferrite powders the majority of the particles have a size above the critical size d_{sp} for superparamagnetism. From Table 1, it can be deduced that d_{sp} is between 5 and 14 nm. The ZFC/FC curves (Fig. 5d) of the ferrite powder obtained at 300 °C are typical of nanocrystalline powders with a significant width of the crystallite size distribution. The ZFC curve displays a hump at T = 80 K indicating a transition to superparamagnetic behavior for some fine particles. Both, FC and ZFC curves are still separated up to 300 K which might be interpreted as being due to a distribution of blocking temperatures T_B pointing again to a larger distribution of particle sizes. The ZFC/FC curves of the ferrite powder obtained at 400 °C do not exhibit the typical features of a superparamagnetic material which is in agreement with the results of the $M(H)$ measurements (Fig. 5c).

Room temperature Mössbauer spectra of the nanocrystalline ferrite powders obtained at 300, 400, and 500 °C are shown in Fig. 6. The spectrum of the ferrite powder prepared at 300 °C (Fig. 6a) shows a doublet structure confirming that the material is superparamagnetic at room temperature. This is consistent with the disappearance of hysteresis in the $M(H)$ curve (Fig. 5c). The doublet can be modeled very well by a superposition of two contributions due to Fe^{3+} ions with different values of the quadrupole splitting. According to their isomeric shifts [33], both quadrupole doublets are due to iron located on sites of octahedral coordination. The spectrum of the ferrite prepared at 400 °C (Fig. 6b) consists of a central doublet (14% intensity) and a magnetically split sextet. The sextet is composed of two contributions with different hyperfine fields which are due to ferric ions on tetrahedral and octahedral sites of the spinel lattice. The Mössbauer spectrum

indicates that the powder consists of a mixture of smaller superparamagnetic particles as well as of larger ferrimagnetic particles. In agreement with that the $M(H)$ curve at 298 K displays a non-zero coercivity. The Mössbauer spectrum of the ferrite prepared at 500 °C (Fig. 6c) is dominated by a sextet with two hyperfine field contributions, i.e. most of the particles display ferrimagnetic behavior. A central doublet of minor intensity (3.5%) is still present indicating that a small fraction of particles is still in the superparamagnetic state. In an alternative interpretation, the central doublet in the spinels synthesized at 400 and 500 °C could be assigned to $ZnFe_2O_4$ which is paramagnetic at room temperature. However, their quadrupole splittings of around 0.6 mm/s, Fig. 6, are almost twice as large as the splitting of 0.33 mm/s observed in $ZnFe_2O_4$ at room temperature [34]. In addition, a splitting of 0.6 mm/s is also found for the superparamagnetic sample prepared at 400 °C. Therefore, the above given interpretation in terms of superparamagnetic contributions to the spectra appears more appropriate.

Comparison of the spectra of the materials prepared at 400 and 500 °C reveals significant differences in the cation distributions of these spinels. In both cases, the sextet structure has been fitted by superposition of two contributions where the one with the larger and well-defined local magnetic field of about 49 T is attributed to Fe^{3+} ions on tetrahedrally coordinated sites. The second contribution due to Fe^{3+} in octahedral coordination is described by a line shape function that accounts for a distribution of local fields at these sites. Most significant, however, is the change in the relative intensities of the two contributions in the two samples showing an increasing preference of iron for the octahedrally coordinated sites with increasing temperature of synthesis. This behavior is also reflected in the lattice parameters of both materials (see above). The lattice constant of the spinel prepared at 500 °C ($a_0 = 8.495(3)$ Å) is typical of a Mn–Zn ferrite with this composition and equilibrium cation distribution, whereas the smaller unit cell length observed for the sample prepared at 400 °C points at an incomplete crystallization of a homogeneous spinel phase or a non-equilibrium cation distribution.

4. Conclusions

Mn–Zn–Fe oxalate hydrate powders were calcined at 300, 400, and 500 °C in air. This results in nanocrystalline spinel ferrite powders with crystallite sizes ranging between 5 and 45 nm. At 500 °C, the spinel ferrite is metastable and transforms into a mixture of haematite/spinel during prolonged annealing in air. The nanosized ferrites undergo a series of phase transformations upon heating in air until at 1180 °C the single-phase Mn–Zn ferrite is re-formed. The magnetization behavior of the ferrite powders is typical of nanocrystalline magnetic particles: the saturation magnetization at 5 K increases with crystallite size and is smaller than that of the bulk ferrites. Hysteretic $M(H)$ behavior is observed for all samples at 5 and 295 K except for the ferrite prepared at 300 °C which is superparamagnetic at room temperature. Room temperature Mössbauer spectroscopy confirms these findings and indicates significant differences in the cation distributions of the investigated samples.

Acknowledgements

The authors acknowledge financial support from the Bundesministerium für Bildung und Forschung (Germany) under the grant Fanimat Nano (03WKF22E).

References

[1] M. Sugimoto, J. Am. Ceram. Soc. 82 (1999) 269–280.
[2] S. Komarneni, E. Fregeau, E. Breval, R. Roy, J. Am. Ceram. Soc. 71 (1988) C26–C28.
[3] M. Rozman, M. Drofenik, J. Am. Ceram. Soc. 78 (1995) 2449–2455.
[4] L. Nalbandian, A. Delimitis, V.T. Zaspalis, E.A. Deliyanni, D.N. Bakoyannakis, E.N. Peleka, Micropor. Mesopor. Mater. 114 (2008) 465–473.
[5] D. Arcos, R. Valenzuela, M. Vasques, M. Vallet-Regi, J. Solid State Chem. 141 (1998) 10–16.
[6] S. Dasgupta, K.B. Kim, J. Ellrich, J. Eckert, J. Manna, J. Alloys Compd. 424 (2006) 13–20.
[7] Z.G. Zheng, X.C. Zhong, Y.H. Zhang, H.Y. Yu, D.C. Zeng, J. Alloys Compd. 466 (2008) 377–382.
[8] J. Fan, F.R. Sale, IEEE Trans. Magn. 32 (1996) 4854–4856.
[9] J. Azadmanjiri, J. Non-Cryst. Solids 353 (2007) 4170–4173.
[10] A.C.F.M. Costa, V.J. Silva, C. Xin, D.A. Vieira, D.R. Cornejoc, R. Kiminami, J. Alloys Compd. 405 (2010) 503–505.
[11] D. Yener, H. Giesche, J. Am. Ceram. Soc. 84 (2001) 1987–1995.
[12] D.S. Mathew, R.S. Juang, Chem. Eng. J. 129 (2007) 51–65.
[13] R. Arulmurugan, B. Jeyadevan, G. Vaidyanathan, S. Sendhilnathan, J. Magn. Magn. Mater. 288 (2005) 470–477.
[14] D.G. Wickham, Inorg. Synth. 9 (1967) 152–156.
[15] M. Bremer, S. Fischer, H. Langbein, W. Töpelmann, H. Scheler, Thermochim. Acta 209 (1992) 323–330.
[16] K.G. Kanade, D.P. Amalnerkar, H.S. Potdar, B.B. Kale, Mater. Chem. Phys. 117 (2009) 187–191.
[17] A. Angermann, J. Töpfer, Ceram. Int., submitted for publication.
[18] R. Deyrieux, A. Peneloux, Bull. Soc. Chim. Fr. 8 (1969) 2675–2681.
[19] A. Angermann, J. Töpfer, J. Mater. Sci. 43 (2008) 5123–5130.
[20] R. Glenn Rupard, P.K. Gallagher, Thermochim. Acta 272 (1996) 11–26.
[21] R.L. Frost, M.L. Weier, J. Therm. Anal. Calorim. 75 (2004) 277–291.
[22] A. Feltz, J. Töpfer, Z. Anorg. Allg. Chem. 576 (1989) 71–80.
[23] J. Töpfer, J. Jung, Thermochim. Acta 202 (1992) 281–289.
[24] K. Lagarec, D.G. Rancourt, Recoil-Mössbauer Spectral Analysis Software for Windows, Version 1.02, Department of Physics, University of Ottawa, Ottawa, Canada, 1998.
[25] R. Morineau, M. Paulus, IEEE Trans. Magn. 11 (1975) 1312–1314.
[26] J. Töpfer, R. Dieckmann, J. Eur. Ceram. Soc. 24 (2004) 603–612.
[27] B. Gillot, M. El Guendouzi, P. Tailhades, A. Rousset, React. Solid 1 (1986) 139–152.
[28] B. Gillot, M. El Guendouzi, Thermochim. Acta 162 (1990) 265–275.
[29] C. Michalk, E. Richter, C. Semmelhack, Hermsdorfer Techn. Mitt 27 (1987) 2253–2257 (in German).
[30] S. Guillemet-Fritsch, S. Viguie, A. Rousset, J. Solid State Chem. 146 (1999) 245–252.
[31] J. Smith, H.P.J. Wijn, Ferrites, Centrex Verlag, Eindhoven, 1962, p. 182 (in German).
[32] V. Sepalak, I. Bergmann, A. Feldhoff, P. Heitjans, F. Krumeich, D. Menzel, F.J. Litterst, S.J. Campbell, K.D. Becker, J. Phys. Chem. C 111 (2007) 5026–5033.
[33] F. Menil, J. Phys. Chem. Solids 46 (1985) 763–789.
[34] V. Sepelak, S. Wissmann, K.D. Becker, J. Mater. Sci. 33 (1998) 2845.